ARTICLE

Adaptive Time Slot Resource Allocation in SWIPT IoT Networks

Yunong Yang[1] , Yuexia Zhang[2,3,*] and Zhihai Zhuo[2]

[1]Key Laboratory of Information and Communication Systems, Ministry of Information Industry, Beijing Information Science and Technology University, Beijing, 100101, China

[2]Key Laboratory of Modern Measurement & Control Technology, Ministry of Education, Beijing Information Science & Technology University, Beijing, 100101, China

[3]Beijing Advanced Innovation Center for Future Blockchain and Privacy Computing, Beijing, 100101, China

*Corresponding Author: Yuexia Zhang. Email: zhangyuexia@bistu.edu.cn

ABSTRACT

The rapid advancement of Internet of Things (IoT) technology has brought convenience to people's lives; however further development of IoT faces serious challenges, such as limited energy and shortage of network spectrum resources. To address the above challenges, this study proposes a simultaneous wireless information and power transfer IoT adaptive time slot resource allocation (SIATS) algorithm. First, an adaptive time slot consisting of periods for sensing, information transmission, and energy harvesting is designed to ensure that the minimum energy harvesting requirement is met while the maximum uplink and downlink throughputs are obtained. Second, the optimal transmit power and channel assignment of the system are obtained using the Lagrangian dual and gradient descent methods, and the optimal time slot assignment is determined for each IoT device such that the sum of the throughput of all devices is maximized. Simulation results show that the SIATS algorithm performs satisfactorily and provides an increase in the throughput by up to 14.4% compared with that of the fixed time slot allocation (FTS) algorithm. In the case of a large noise variance, the SIATS algorithm has good noise immunity, and the total throughput of the IoT devices obtained using the SIATS algorithm can be improved by up to 34.7% compared with that obtained using the FTS algorithm.

KEYWORDS

Internet of Things; simultaneous wireless information and power transfer; adaptive; time slot; resource allocation

1 Introduction

With the continuous development in communication technology, Internet of Things (IoT) has been gradually integrated into many aspects of public life (e.g., public safety, smart city, enemy reconnaissance, and many other fields) [1–6]. According to statistics, the number of Internet of Things devices (IoDs) may reach 30 billion by 2025. The widespread application of IoT enables the communication between people and things and among things at any time and place [7,8]. In addition to increasing convenience, it also promotes intelligence development in public life. Thus, the proliferation of IoT has greatly improved the quality of life, and it is of great practical significance to study IoT.

Although IoT has become an irreplaceable part of public life, the IoT system faces challenges, such as limited energy storage of the IoDs and the scarcity of spectrum resources [9]. The emergence of simultaneous wireless information and power transfer (SWIPT) technology has provided a new method of solving the problem of the limited energy of the IoDs [10]. The application of the SWIPT technology allows IoDs to harvest energy from radio frequency (RF) waves and convert it into electrical energy, which can be stored in the battery of the device, thus maximizing the usable time of the device [11,12] and reducing the additional cost of battery replacement or manual charging of the device [13]. However, there is a limit to the amount of energy that can be stored in the battery, and excessive energy harvesting puts a greater burden on the operation of the device. Less than the appropriate amount of energy disrupts the normal operation of the device, and adequate energy harvesting using SWIPT IoT enables the entire network system to continue operating. Meanwhile, the normal communication of IoDs requires the support of large amounts of the radio spectrum, and the recent shortage of spectrum resources has restricted the development of IoT [14]. Therefore, reasonable allocation of the limited spectrum resources has become the focus of research in regard to SWIPT IoT.

A number of recent studies have considered the issue of resource allocation in regard to energy harvesting in SWIPT IoT. Zhu et al. [15] determined the user maximized minimum energy harvesting subject to the secrecy rate and total transmit power constraints in the presence of channel estimation errors, ensuring the fairness of user energy harvesting. Masood et al. [16] proposed an algorithm to achieve a compromise between energy efficiency and spectral efficiency in the SWIPT system, which is based on using the Lagrange multiplier method to find the optimal solution without iterative computation. Simulation results proved that the algorithm achieved the maximum energy transmission by using the optimal power split ratio. Han et al. [17] studied fair resource allocation in terms of the maximum–minimum energy requirement for wireless power transmission in edge computing systems. They solved the nonconvex mixed-integer nonlinearity that arises when using a logarithmic nonlinear energy harvesting model by using a continuous relaxation method. Yazdani et al. [18] proposed a parametric power control method that allows each sub-user to adjust its power according to the stored energy such that the lower limit of the sum of the uplink rates is maximized. Xu et al. [19] studied the resource allocation problem with perfect channel state information under the constraints of minimum energy harvesting and quality of service. Qi et al. [20] considered channel uncertainty, receiver nonlinearity, and decoding message cancellation for imperfect continuous messages in SWIPT-based non-orthogonal multiple access (NOMA) large scale IoT in the process of designing a resource allocation method.

Researchers have also considered joint optimization and allocation of multiple resources in SWIPT IoT. Prathima et al. [21] considered a collaborative cognitive radio (CR) network with two primary and secondary users, wherein power splitting and time-switching energy harvesting techniques were used and the system throughput and energy efficiency were maximized by using a particle swarm optimization algorithm. Acosta et al. [22] jointly considered the energy harvesting of the system, data rate, and the maximum power level allowed to interfere with the users to minimize the transmit power of the auxiliary base station. They solved the external and internal optimizations using a particle swarm optimization algorithm and a semidefinite relaxation algorithm, respectively. Tuan et al. [23] investigated resource allocation with respect to maximizing the total energy harvesting and energy harvesting efficiency under linear and nonlinear energy harvesting models in a SWIPT system consisting of a multi-input single-output interference channel to jointly optimize the beam formation vector of the transmitter and the power splitting ratio of the receiver. Hu et al. [24] maximized the secrecy rate in a multi-input multi-output bidirectional relay-assisted CR NOMA

network by jointly optimizing the power allocation of the users and power splitting factor under the constraints of quality of service, energy harvesting, and transmission power. Tang et al. [25] jointly optimized the transmission rate and harvested energy in a SWIPT-enabled NOMA system using power splitting to simultaneously fulfill the minimum rate and harvested energy requirements for each user. Yang et al. [26] used resource management methods based on deep reinforcement learning to jointly optimize radio allocation and control strategies of transmission power in cognitive IoT. Ramzan et al. [27] simultaneously optimized device selection, unmanned aerial vehicle (UAV) relay allocation, and power splitting ratio in an IoT system based on UAV relay communication with energy harvesting, where the optimization results showed significant advantages in the above aspects. Xiao et al. [28] maximized the energy efficiency in RF energy-driven CR networks by jointly optimizing transmission time and power control and also proposed a resource allocation scheme called the co-channel interference approximation convex strategy. These studies investigated resource allocation in regard to SWIPT IoT and obtained adequate results. However, most researchers only focused on the uplink or downlink information transmission in SWIPT IoT systems without considering that most IoDs required alternating uplink and downlink information transmissions in real-time. This problem can be addressed by jointly allocating resources for uplink and downlink information transmissions and energy harvesting in SWIPT IoT such that the results obtained can be more in line with actual situations.

The main contributions of this study are summarized as follows:

- An adaptive time slot (ATS) structure is designed that consists of a sensing time period at the beginning, time periods for several alternating uplink and downlink information transmissions, and a common time period for downlink energy harvesting and information transmission. The ATS structure allows the IoD to adaptively allocate time in a time slot to obtain the maximum uplink and downlink throughputs while satisfying the minimum energy harvesting requirements.

- A SWIPT IoT ATS resource allocation (SIATS) algorithm is proposed. The algorithm first solves the coupling problem in the optimization function by using the method of pre-setting sensing time, time allocation factor, and time slot allocation parameters and transforms the optimization function into a convex function. Second, the optimal transmit power and channel assignment of the system is obtained by using the Lagrangian dual and gradient descent methods. Finally, by comparing the throughput results with different sensing times, time allocation factors, and time slot allocation parameters, the optimal time slot allocation for each IoD is determined such that the sum of the throughputs of all IoDs in the system is maximized.

- The simulation compares the system throughput and energy harvesting when using the SIATS algorithm proposed in this paper with the fixed time slot allocation (FTS) algorithm, and analyzes in detail the effects of parameters such as sensing time, time allocation factor, and noise on the total system throughput and energy harvesting.

2 System Model

The SWIPT IoT network system is shown in Fig. 1, and it is composed of B IoT base stations, denoted as $BS_1, BS_2, \ldots, BS_B$. Each base station possesses a certain communication range and can communicate with and provide energy to the IoDs within its communication range in real-time. Each IoD is equipped with an antenna, an energy harvesting module, and a battery that can be charged with the power provided by the energy harvesting module.
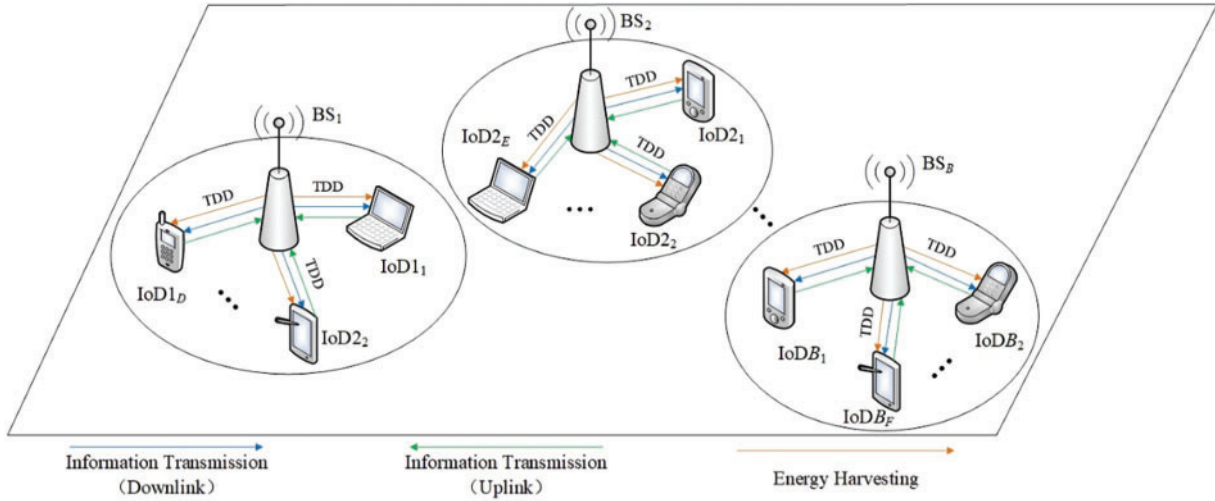
Figure 1: SWIPT IoT network system

The spectrum resources of the SWIPT IoT network system are divided into C available channels, denoted by the set $\mathbb{C} = \{CH_1, CH_2, \ldots, CH_j, \ldots, CH_C\}$. The IoT base stations in this network can sense the available spectrum resources to ensure that different frequencies are used for the IoDs in their respective coverage areas. Let us suppose that the communication range of BS_1 contains D IoDs, denoted by the set $\mathbb{D} = \{IoD1_1, IoD1_2, \ldots, IoD1_i, \ldots, IoD1_D\}$, where $IoD1_i$ denotes the ith IoD in the communication range of BS_1. The communication range of BS_2 contains E IoDs, denoted by the set $\mathbb{E} = \{IoD2_1, IoD2_2, \ldots, IoD2_i, \ldots, IoD2_E\}$, where $IoD2_i$ denotes the ith IoD in the communication range of BS_2.

The communication mode between the IoT base station and IoD is the time division duplex, for which an ATS structure is designed, as shown in Fig. 2.
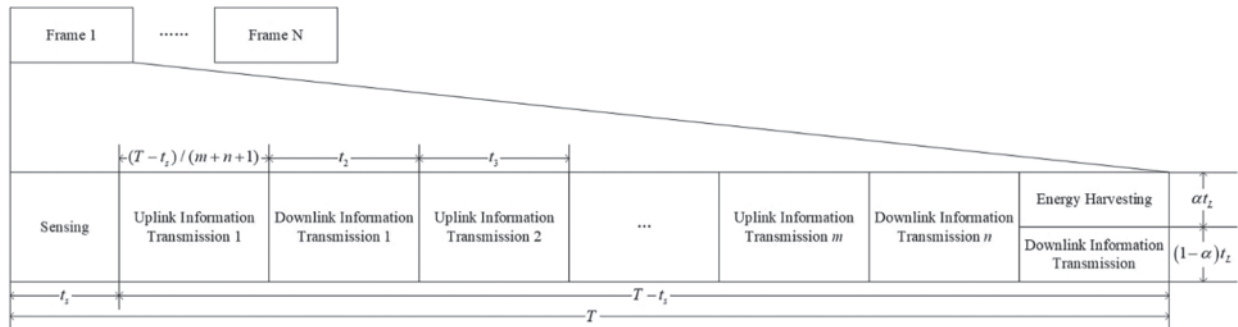
Figure 2: Adaptive time slot structure

The ATS consists of periods for sensing, uplink information transmission, downlink information transmission, and energy harvesting. The total duration of the time slot is T, where the first time period is used for sensing, and the duration is t_s. The subsequent $T - t_s$ durations are divided into L time periods of equal length, which can be denoted as $t_1, t_2, \ldots, t_{L-1}, t_L$. The time periods t_1 to t_{L-1} are primarily used for information transmission, where m time periods are used for the uplink information transmission and n time periods are used for the downlink information transmission, and the values

of m and n in a time slot are determined adaptively. Thus, the duration of the uplink information transmission in time periods t_1 to t_{L-1} can be calculated by the following equation:

$$T_u = m \frac{T - t_s}{m + n + 1} \tag{1}$$

Furthermore, the duration of the downlink information transmission in the time period t_1 to t_{L-1} can be calculated by the following equation:

$$T_{o,d} = n \frac{T - t_s}{m + n + 1} \tag{2}$$

The time period t_L in the time slot is the common time for energy harvesting and downlink information transmission. The time period t_L is split by a time allocation factor $\alpha \in [0, 1]$. This parameter varies with the channel conditions and IoD requirements in different time slots. Thus, the duration of time to perform energy harvesting in time period t_L can be calculated as:

$$T_{c,e} = \alpha \frac{T - t_s}{m + n + 1} \tag{3}$$

The duration of time for the downlink information transmission is calculated as:

$$T_{c,d} = (1 - \alpha) \frac{T - t_s}{m + n + 1} \tag{4}$$

Finally, the duration of the complete time slot for the downlink information transmission is calculated as:

$$T_d = T_{o,d} + T_{c,d} = (n + 1 - \alpha) \frac{T - t_s}{m + n + 1} \tag{5}$$

The following is an illustration of the IoT SWIPT network communication considering the IoT base station BS_1 as an example; let us assume BS_1 and BS_2 are adjacent base stations, as shown in Fig. 1. Each IoD within the communication range of BS_1 senses the state of all channels at the beginning of each time slot, and the results of the sensing are categorized into two cases.

(1) The first case: The IoD within the communication range of BS_1 senses that the channel is idle. The channel is not used by the IoD within the communication range of BS_1, and it is also not used by the IoD within the adjacent base station BS_2. The probability of this case is assumed to be p_j^{true}.

(2) The second case: The IoD within the communication range of BS_1 senses the channel is idle. The channel is not used by the IoD within the communication range of BS_1, but it is used by the IoD within the neighboring base station BS_2. The probability of this case is assumed to be p_j^{false}.

The two cases are discussed separately in the following section.

2.1 The First Case

Based on the previous assumptions, the probability p_j^{true} is computed as:

$$p_j^{true} = p \left(H_j (0) \right) \left(1 - p_{error,j} (t_s) \right), \tag{6}$$

where $p \left(H_j (0) \right)$ denotes the probability that CH_j is idle and $p_{error,j}$ denotes the probability of a false alarm for CH_j, which can be computed as follows:

$$p_{error,j} (t_s) = F \left(\sqrt{2SNR_j + 1} \cdot F^{-1} (p_p) + \sqrt{t_s f_s} SNR_j \right), \tag{7}$$

where SNR_j denotes the signal-to-noise ratio of the signal received by the IoD using CH_j communication, f_s denotes the sampling frequency of the signal, and $F(\cdot)$ denotes the standard Gaussian complementary cumulative distribution function, which can be expressed as follows:

$$F(x) = \int_x^\infty \frac{1}{\sqrt{2\pi}} e^{\left(-\frac{t^2}{2}\right)} dt \tag{8}$$

Notably, $F^{-1}(\cdot)$ is the inverse function of $F(\cdot)$.

The IoD within the communication range of BS_1 selects one or more available channels to communicate with BS_1 after the sensing, and this system ensures that one channel is available for each IoD. During the communication process between BS_1 and the IoD, the uplink is primarily used to transmit the information from the IoD to BS_1.

The rate of transmission corresponding to $IoD1_i$ for the uplink information transmission using CH_j in this case can be determined using Shannon's formula, as follows:

$$r_{i,j}^{true}(T_u) = W \log_2 \left(1 + \frac{P_{i,j,u}^1 h_{i,j}}{N}\right), \tag{9}$$

where the superscript *true* in $r_{i,j}^{true}$ denotes the first case; the subscript i represents the device $IoD1_i$, and the subscript j represents the channel CH_j used by the device. $P_{i,j,u}^1$ denotes the transmit power of $IoD1_i$ when using CH_j for the uplink information transmission, where the superscript 1 denotes the communication range of BS_1 the subscript i denotes $IoD1_i$, the subscript j denotes CH_j used by the device, and the subscript u indicates uplink information transmission. In the above equation, W denotes the channel bandwidth, $h_{i,j}$ denotes the channel gain for communication between BS_1 and $IoD1_i$ using CH_j, and N denotes the variance of the additive Gaussian white noise.

The downlink in the communication process is primarily used to send data from BS_1 to the IoD within its communication range and to provide energy to the IoD when needed. Thus, the rate of transmission for the downlink information transmission between $IoD1_i$ and BS_1 using CH_j is computed as:

$$r_{i,j}^{true}(T_d) = W \log_2 \left(1 + \frac{P_{i,j,d}^1 h_{i,j}}{N}\right), \tag{10}$$

where $P_{i,j,d}^1$ denotes the transmit power for the downlink information transmission between BS_1 and $IoD1_i$ using CH_j, wherein the subscript d indicates downlink information transmission.

2.2 The Second Case

Based on the previous assumptions, the probability p_j^{false} is computed as:

$$p_j^{false} = p\left(H_j(1)\right)\left(1 - p_p\right), \tag{11}$$

where $p\left(H_j(1)\right)$ is the probability that CH_j is busy and $p\left(H_j(1)\right) = 1 - p\left(H_j(0)\right)$. p_p is the probability of target detection that adequately protects the IoD.

In this case, the signal emitted by BS_2 during the uplink information transmission with $IoD2_i$ interferes with the uplink information transmission using the co-channel within the communication range of BS_1. Therefore, the rate of transmission corresponding to $IoD1_i$ during the uplink information transmission using CH_j is computed as:

$$r_{i,j}^{false}(T_u) = W \log_2 \left(1 + \frac{P_{i,j,u}^1 h_{i,j}}{P_{i,j,u}^2 g_{i,j} + N}\right), \tag{12}$$

where the superscript *false* in $r_{i,j}^{false}$ denotes the second case. $P_{i,j,u}^2$ denotes the transmit power received by BS_1 when $IoD2_i$ uses the co-channel of CH_j for the uplink information transmission; the superscript 2 denotes the communication range of BS_2, the subscript i denotes the device $IoD2_i$, the subscript j denotes the co-channel of CH_j, and the subscript u indicates uplink information transmission. Additionally, $g_{i,j}$ denotes the channel gain for communication between $IoD2_i$ and BS_1 performed using the co-channel of CH_j.

The uplink interference generated by $IoD1_i$ and BS_1 using CH_j for the uplink information transmission to $IoD2_i$ within the communication range of BS_2 using the co-channel of CH_j can be computed as:

$$I_{j,u} = \frac{T_u}{T} p_j^{false} \sum_{i=1}^{D} l_{i,j} P_{i,j,u}^1 \phi_{i,j}, \tag{13}$$

where $l_{i,j}$ is the channel gain for communication between $IoD1_i$ to BS_2 performed using the co-channel of CH_j. $\phi_{i,j} = \{0, 1\}$ is used to indicate whether $IoD1_i$ uses CH_j, and it is called the channel assignment factor. When $IoD1_i$ uses CH_j, $\phi_{i,j} = 1$; conversely, $\phi_{i,j} = 0$.

The uplink throughput of $IoD1_i$ on CH_j can be expressed as:

$$r_{i,j,u} = \frac{T_u}{T} \left[p_j^{true} r_{i,j}^{true} (T_u) + p_j^{false} r_{i,j}^{false} (T_u) \right] \tag{14}$$

The rate of transmission for the downlink information transmission between $IoD1_i$ and BS_1 performed using CH_j is computed as:

$$r_{i,j}^{false} (T_d) = W \log_2 \left(1 + \frac{P_{i,j,d}^1 h_{i,j}}{P_{i,j,d}^2 l_{i,j} + N} \right), \tag{15}$$

where $P_{i,j,d}^2$ denotes the transmit power of BS_2 when the co-channel of CH_j is used for the downlink information transmission.

The downlink interference generated by BS_1 and $IoD1_i$ using CH_j for the downlink information transmission to BS_2 using the co-channel of CH_j can be computed as:

$$I_{j,d} = \frac{T_d}{T} p_j^{false} \sum_{i=1}^{D} g_{i,j} P_{i,j,d}^1 \phi_{i,j} \tag{16}$$

The downlink throughput can be expressed as:

$$r_{i,j,d} = \frac{T_d}{T} \left[p_j^{true} r_{i,j}^{true} (T_d) + p_j^{false} r_{i,j}^{false} (T_d) \right] \tag{17}$$

2.3 Energy Harvesting

For energy harvesting in the downlink, a linear energy harvesting model is used in this study. Thus, the energy harvested by $IoD1_i$ using CH_j can be expressed as:

$$E_{i,j} = \beta \frac{T_{c,e}}{T} \left[h_{i,j} \left(p_j^{true} + p_j^{false} \right) P_{i,j,d}^1 + N \right] \phi_{i,j}, \tag{18}$$

where β is the energy efficiency conversion constant, and $\beta \in [0, 1]$.

It is assumed in this study that the IoD can simultaneously use more than one channel to communicate with the base station. Therefore, the total energy harvested by IoD1$_i$ in a time slot can be expressed as:

$$E_i = \sum_{j=1}^{C} E_{i,j} \tag{19}$$

3 SWIPT IoT ATS Resource Allocation Algorithm

In order to achieve an optimal system, a joint optimization is performed to maximize the sum of the uplink and downlink throughputs of all IoDs within the communication range of BS$_1$. This optimization problem can be stated as follows:

$$\max \sum_{i=1}^{D} \sum_{j=1}^{C} \phi_{i,j} \left(r_{i,j,u} + r_{i,j,d} \right) \tag{20a}$$

$$s.t. \frac{T_d}{T} p_j^{false} \sum_{i=1}^{D} g_{i,j} P_{i,j,d}^1 \phi_{i,j} \leq I_{\max,j,d}, j \in \mathbb{C} \tag{20b}$$

$$\frac{T_u}{T} p_j^{false} \sum_{i=1}^{D} l_{i,j} P_{i,j,u}^1 \phi_{i,j} \leq I_{\max,j,u}, j \in \mathbb{C} \tag{20c}$$

$$\frac{T_d}{T} \sum_{i=1}^{D} \sum_{j=1}^{C} \left(p_j^{true} + p_j^{false} \right) P_{i,j,d}^1 \phi_{i,j} \leq P_{\max,d} \tag{20d}$$

$$\frac{T_u}{T} \sum_{j=1}^{C} \left(p_j^{true} + p_j^{false} \right) P_{i,j,u}^1 \phi_{i,j} \leq P_{\max,i,u}, i \in \mathbb{D} \tag{20e}$$

$$\sum_{j=1}^{C} \beta \frac{T_{c,e}}{T} \phi_{i,j} \left[h_{i,j} \left(p_j^{true} + p_j^{false} \right) P_{i,j,d}^1 + N \right] \geq E_{\min,i}, i \in \mathbb{D} \tag{20f}$$

$$\sum_{i=1}^{D} \phi_{i,j} = 1, j \in \mathbb{C} \tag{20g}$$

$$0 < t_s \leq T \tag{20h}$$

$$0 < \alpha \leq 1 \tag{20i}$$

$$\phi_{i,j} = \{0, 1\}, i \in \mathbb{D}, j \in \mathbb{C} \tag{20j}$$

$$P_{i,j,u}^1 \geq 0, i \in \mathbb{D}, j \in \mathbb{C} \tag{20k}$$

$$P_{i,j,d}^1 \geq 0, i \in \mathbb{D}, j \in \mathbb{C} \tag{20l}$$

Here, $I_{\max,j,d}$ denotes the maximum acceptable downlink interference in the communication range of BS$_2$, $I_{\max,j,u}$ denotes the maximum acceptable uplink interference in the communication range of BS$_2$,

$P_{\text{max},d}$ is the maximum value of the transmit power of BS_1, $P_{\text{max},i,u}$ is the maximum value of the transmit power of $IoD1_i$ and $E_{\text{min},i}$ is the minimum energy to be harvested by $IoD1_i$ in the time slot.

In this optimization problem, the constraint represented by Eq. (20b) indicates that the interference of the downlink information transmission within the communication range of BS_1 to the downlink information transmission in BS_2 using the co-channel is less than the maximum acceptable threshold for downlink interference. The constraint represented by Eq. (20c) indicates that the interference of the uplink information transmission within the communication range of BS_1 to the uplink information transmission in BS_2 using the co-channel is less than the maximum acceptable threshold for uplink interference. The constraint represented by Eq. (20d) indicates that the sum of the power transmitted by BS_1 to the IoD within its communication range is less than the maximum transmit power of the base station. The constraint represented by Eq. (20e) indicates that the sum of the transmit power of each IoD for the uplink information transmission over the available channel is less than the maximum transmit power of the device. The constraint represented by Eq. (20f) indicates that the sum of the energy harvested by each IoD through its available channels is greater than the minimum energy harvesting requirement. The constraint represented by Eq. (20g) indicates that each channel cannot be used by more than one IoD. The constraint represented by Eq. (20h) provides the range of values for sensing time. The constraint represented by Eq. (20i) provides the range of values for the time allocation factor; The constraint in Eq. (20j) provides the range of values for the channel allocation factor. Finally, the constraints in Eqs. (20k) and (20l) ensure that neither the uplink nor downlink transmit power is less than zero.

To solve the optimization problem, a SIATS algorithm is proposed in this study that can be described as follows.

The channel assignment factor $\phi_{i,j} = \{0, 1\}$ in Eqs. (20a)–(20g) renders the original optimization problem a mixed-integer programming problem, which causes the original problem to become intractable. Therefore, the value of the channel assignment factor $\phi_{i,j}$ can be relaxed as $\phi_{i,j} = [0, 1]$ in the derivation process. In this study, we introduce the auxiliary variables $\varphi_{i,j,d} = \phi_{i,j} P^1_{i,j,d}$, $\varphi_{i,j,u} = \phi_{i,j} P^1_{i,j,u}$, which can be incorporated into Eqs. (9), (10), (12), and (15) to obtain the following four equations:

$$r^{true}_{i,j}(T_u) = W \log_2\left(1 + \frac{\varphi_{i,j,u} h_{i,j}}{\phi_{i,j} N}\right) \tag{21}$$

$$r^{true}_{i,j}(T_d) = W \log_2\left(1 + \frac{\varphi_{i,j,d} h_{i,j}}{\phi_{i,j} N}\right) \tag{22}$$

$$r^{false}_{i,j}(T_u) = W \log_2\left(1 + \frac{\varphi_{i,j,u} h_{i,j}}{\phi_{i,j}\left(P^2_{i,j,u} g_{i,j} + N\right)}\right) \tag{23}$$

$$r^{false}_{i,j}(T_d) = W \log_2\left(1 + \frac{\varphi_{i,j,d} h_{i,j}}{\phi_{i,j}\left(P^2_{i,j,d} l_{i,j} + N\right)}\right) \tag{24}$$

According to Eqs. (14) and (17), the optimization objective Eq. (20a) can be expressed as:

$$\psi = \sum_{i=1}^{D} \sum_{j=1}^{C} \phi_{i,j} \left\{ \frac{T_u}{T}\left[p^{true}_j r^{true}_{i,j}(T_u) + p^{false}_j r^{false}_{i,j}(T_u)\right] + \frac{T_d}{T}\left[p^{true}_j r^{true}_{i,j}(T_d) + p^{false}_j r^{false}_{i,j}(T_d)\right]\right\} \tag{25}$$

Subsequently, upon incorporating Eqs. (21)–(24) into the optimization problem in Eq. (20), it can be transformed into the formulation expressed by Eqs. (26a)–(26n):

$$\max \psi \tag{26a}$$

$$s.t. \frac{T_d}{T} p_j^{false} \sum_{i=1}^{D} g_{i,j} \varphi_{i,j,d} \leq I_{\max,j,d}, j \in \mathbb{C} \tag{26b}$$

$$\frac{T_u}{T} p_j^{false} \sum_{i=1}^{D} l_{i,j} \varphi_{i,j,u} \leq I_{\max,j,u}, j \in \mathbb{C} \tag{26c}$$

$$\frac{T_d}{T} \sum_{i=1}^{D} \sum_{j=1}^{C} \left(p_j^{true} + p_j^{false} \right) \varphi_{i,j,d} \leq P_{\max,d} \tag{26d}$$

$$\frac{T_u}{T} \sum_{j=1}^{C} \left(p_j^{true} + p_j^{false} \right) \varphi_{i,j,u} \leq P_{\max,i,u}, i \in \mathbb{D} \tag{26e}$$

$$\sum_{j=1}^{C} \beta \frac{T_{c,e}}{T} \left[h_{i,j} \left(p_j^{true} + p_j^{false} \right) \varphi_{i,j,d} + \phi_{i,j} N \right] \geq E_{\min,i}, i \in \mathbb{D} \tag{26f}$$

$$\sum_{i=1}^{D} \phi_{i,j} = 1, j \in \mathbb{C} \tag{26g}$$

$$0 < t_s \leq T \tag{26h}$$

$$0 < \alpha \leq 1 \tag{26i}$$

$$0 \leq \phi_{i,j} \leq 1, i \in \mathbb{D}, j \in \mathbb{C} \tag{26j}$$

$$P_{i,j,u}^1 \geq 0, i \in \mathbb{D}, j \in \mathbb{C} \tag{26k}$$

$$P_{i,j,d}^1 \geq 0, i \in \mathbb{D}, j \in \mathbb{C} \tag{26l}$$

$$\varphi_{i,j,u} \geq 0, i \in \mathbb{D}, j \in \mathbb{C} \tag{26m}$$

$$\varphi_{i,j,d} \geq 0, i \in \mathbb{D}, j \in \mathbb{C} \tag{26n}$$

In this optimization problem, the constraints in Eqs. (26m) and (26n) ensure that the auxiliary variables are not less than zero. The reason for adding these two constraints is that the auxiliary variables are calculated by multiplying the transmit power and the channel assignment factor, while the transmit power takes a value greater than or equal to 0 and the channel assignment factor takes a value between 0 and 1. Therefore, the auxiliary variables also need to comply with the condition that they are not less than zero. The optimization problem expressed by Eqs. (26a)–(26n) is a nonconvex problem, and a coupling exists between the sensing time t_s, time allocation factor α, time slot allocation

parameters m and n, and auxiliary variables $\varphi_{i,j,u}$ and $\varphi_{i,j,d}$. Therefore, the optimal solutions t_s^*, α^*, m^*, and n^* can be solved by using the method of predetermined values, and the optimization problem presented in Eqs. (26a)–(26n) is transformed into a convex optimization problem using the four determined parameters t_s, α, m, and n. This study uses the dual gradient descent method to address the convex optimization problem with the given parameters. The problem formulated by Eqs. (26a)–(26n) is transformed into a dual problem using a Lagrangian function, which is expressed as Eq. (27), where λ_j, χ_j, ω, θ_i, ϑ_i, and ξ_j are the Lagrangian variables.

$$
L\left(\varphi_{i,j,u}, \varphi_{i,j,d}, \phi_{i,j}; \lambda_j, \chi_j, \omega, \theta_i, \vartheta_i, \xi_j\right) = \psi + \sum_{j=1}^{C} \lambda_j \left(I_{\max,j,d} - \frac{T_d}{T} p_j^{false} \sum_{i=1}^{D} g_{i,j} \varphi_{i,j,d} \right)
$$

$$
+ \sum_{j=1}^{C} \chi_j \left(I_{\max,j,u} - \frac{T_u}{T} p_j^{false} \sum_{i=1}^{D} l_{i,j} \varphi_{i,j,u} \right) + \omega \left[P_{\max,d} - \frac{T_d}{T} \sum_{i=1}^{D} \sum_{j=1}^{C} \left(p_j^{true} + p_j^{false} \right) \varphi_{i,j,d} \right] + \sum_{j=1}^{C} \xi_j \left(1 - \sum_{i=1}^{D} \phi_{i,j} \right)
$$

$$
+ \sum_{i=1}^{D} \theta_i \left[P_{\max,i,u} - \frac{T_u}{T} \sum_{j=1}^{C} \left(p_j^{true} + p_j^{false} \right) \varphi_{i,j,u} \right] + \sum_{i=1}^{D} \vartheta_i \left[\sum_{j=1}^{C} \beta \frac{T_{c,e}}{T} \left(h_{i,j} \left(p_j^{true} + p_j^{false} \right) \varphi_{i,j,d} + N \phi_{i,j} \right) - E_{\min,i} \right]
$$

$$
\tag{27}
$$

The problem, as described by Eqs. (26a)–(26n) can be transformed into a dual problem, which can be expressed as follows:

$$
\min_{\lambda_j, \omega, \theta_i, \vartheta_i, \xi_j \geq 0} f\left(\lambda_j, \chi_j, \omega, \theta_i, \vartheta_i, \xi_j\right), \tag{28}
$$

where

$$
f\left(\lambda_j, \chi_j, \omega, \theta_i, \vartheta_i, \xi_j\right) = \max L\left(\varphi_{i,j,d}, \varphi_{i,j,u}, \phi_{i,j}; \lambda_j, \chi_j, \omega, \theta_i, \vartheta_i, \xi_j\right) \tag{29}
$$

According to the principle of the Karush–Kuhn–Tucker (KKT) condition, the partial derivative of the Lagrangian function with respect to $\varphi_{i,j,u}$ satisfies the following conditions:

$$
\frac{\partial L}{\partial \varphi_{i,j,u}} \begin{cases} = 0 & \varphi_{i,j,u}^* > 0 \\ < 0 & \varphi_{i,j,u}^* < 0 \end{cases}, \tag{30}
$$

where x^* represents the optimal solution for x.

$r_{i,j}^{true}(T_u)$ and $r_{i,j}^{false}(T_u)$ in the Lagrangian function are related to $\varphi_{i,j,u}$. The derivatives of the above two functions with respect to $\varphi_{i,j,u}$ can be expressed as:

$$
\begin{aligned}
\frac{\partial r_{i,j}^{true}(T_u)}{\partial \varphi_{i,j,u}} &= W \frac{h_{i,j}}{\ln 2 \left(\phi_{i,j} N_{i,j,u} + \varphi_{i,j,u} h_{i,j,u} \right)} \\
\frac{\partial r_{i,j}^{false}(T_u)}{\partial \varphi_{i,j,u}} &= W \frac{h_{i,j}}{\ln 2 \left(\phi_{i,j} \left(P_{i,j,u}^2 g_{i,j} + N \right) + \varphi_{i,j,u} h_{i,j} \right)}
\end{aligned} \tag{31}
$$

The partial derivative of Lagrangian function with respect to $\varphi_{i,j,u}$ be expressed as:

$$
\frac{\partial L}{\partial \varphi_{i,j,u}} = \phi_{i,j} \frac{T_u}{T} \left[p_j^{true} W \frac{h_{i,j}}{\ln 2 \left(\phi_{i,j} N + \varphi_{i,j,u} h_{i,j} \right)} + p_j^{false} W \frac{h_{i,j}}{\ln 2 \left(\phi_{i,j} \left(P_{i,j,u}^2 g_{i,j} + N \right) + \varphi_{i,j,u} h_{i,j} \right)} \right]
$$

$$
- \theta_i \frac{T_u}{T} \left(p_j^{true} + p_j^{false} \right) - \chi_j \frac{T_u}{T} p_j^{false} l_{i,j} \tag{32}
$$

For $\dfrac{\partial L}{\partial \varphi_{i,j,u}} = 0$, the optimal solution $\varphi_{i,j,u}^*$ can be obtained by using the quadratic formula. According to the definition of the auxiliary variables, the optimal uplink transmit power can be obtained by using the condition: $P_{i,j,u}^{1*} = \varphi_{i,j,u}^*/\phi_{i,j}$.

According to the principle of the KKT condition, the partial derivative of the Lagrangian function with respect to $\varphi_{i,j,d}$ satisfies the following conditions:

$$\frac{\partial L}{\partial \varphi_{i,j,d}} \begin{cases} = 0 & \varphi_{i,j,d}^* > 0 \\ < 0 & \varphi_{i,j,d}^* < 0 \end{cases} \tag{33}$$

Furthermore, $r_{i,j}^{true}(T_d)$ and $r_{i,j}^{false}(T_d)$ in the Lagrangian function are related to $\varphi_{i,j,d}$. Thus, the derivatives of the above two functions with respect to $\varphi_{i,j,d}$ can be expressed as:

$$\frac{\partial r_{i,j}^{true}(T_d)}{\partial \varphi_{i,j,d}} = W \frac{h_{i,j}}{\ln 2 \left(\phi_{i,j} N + \varphi_{i,j,d} h_{i,j}\right)}$$

$$\frac{\partial r_{i,j}^{false}(T_d)}{\partial \varphi_{i,j,d}} = W \frac{h_{i,j}}{\ln 2 \left(\phi_{i,j} \left(P_{i,j,d}^2 l_{i,j} + N\right) + \varphi_{i,j,d} h_{i,j}\right)} \tag{34}$$

The partial derivative of L with respect to $\varphi_{i,j,d}$ be expressed as:

$$\frac{\partial L}{\partial \varphi_{i,j,d}} = \phi_{i,j} \frac{T_d}{T} \left[p_j^{true} W \frac{h_{i,j}}{\ln 2 \left(\phi_{i,j} N + \varphi_{i,j,d} h_{i,j}\right)} + p_j^{false} W \frac{h_{i,j}}{\ln 2 \left(\phi_{i,j} \left(P_{i,j,d}^2 l_{i,j} + N\right) + \varphi_{i,j,d} h_{i,j}\right)} \right]$$

$$+ \left(p_j^{true} + p_j^{false}\right) \left(\vartheta_i \beta h_{i,j} \frac{T_{c,e}}{T} - \omega \frac{T_d}{T}\right) - \lambda_j \frac{T_d}{T} p_j^{false} g_{i,j} \tag{35}$$

For $\dfrac{\partial L}{\partial \varphi_{i,j,d}} = 0$, the optimal solution $\varphi_{i,j,d}^*$ can be obtained by using the quadratic formula. According to the definition of the auxiliary variables, the optimal uplink transmit power can be obtained by using the condition: $P_{i,j,d}^{1*} = \varphi_{i,j,d}^*/\phi_{i,j}$.

According to the principle of the KKT condition, the partial derivative of the Lagrangian function with respect to $\phi_{i,j}$ satisfies the following conditions:

$$\frac{\partial L}{\partial \phi_{i,j}} \begin{cases} < 0 & \phi_{i,j}^* = 0 \\ = 0 & 0 < \phi_{i,j}^* < 1 \\ > 0 & \phi_{i,j}^* = 1 \end{cases} \tag{36}$$

$r_{i,j}^{true}(T_u)$, $r_{i,j}^{false}(T_u)$, $r_{i,j}^{true}(T_d)$, and $r_{i,j}^{false}(T_d)$ in the Lagrangian function are related to $\phi_{i,j}$. Therefore, the derivatives of the above four functions with respect to $\phi_{i,j}$ can be expressed as:

$$\frac{\partial r_{i,j}^{true}(T_d)}{\partial \phi_{i,j}} = -\frac{W \varphi_{i,j,d} h_{i,j}}{\ln 2 \left(N \phi_{i,j}^2 + \varphi_{i,j,d} h_{i,j} \phi_{i,j}\right)}$$

$$\frac{\partial r_{i,j}^{false}(T_d)}{\partial \phi_{i,j}} = -\frac{W \varphi_{i,j,d} h_{i,j}}{\ln 2 \left(\left(P_{i,j,d}^2 l_{i,j} + N\right) \phi_{i,j}^2 + \varphi_{i,j,d} h_{i,j} \phi_{i,j}\right)}$$

$$\frac{\partial r_{i,j}^{true}(T_u)}{\partial \phi_{i,j}} = -\frac{W \varphi_{i,j,u} h_{i,j}}{\ln 2 \left(N_{i,j,u} \phi_{i,j}^2 + \varphi_{i,j,u} h_{i,j,u} \phi_{i,j}\right)}$$

$$\frac{\partial r_{i,j}^{false}(T_u)}{\partial \phi_{i,j}} = -\frac{W \varphi_{i,j,u} h_{i,j}}{\ln 2 \left(\left(P_{i,j,u}^2 g_{i,j} + N\right) \phi_{i,j}^2 + \varphi_{i,j,u} h_{i,j} \phi_{i,j}\right)} \tag{37}$$

The partial derivative of the L with respect to $\phi_{i,j}$ be expressed as:

$$\frac{\partial L}{\partial \phi_{i,j}} = \frac{T_u}{T}\left[p_j^{true}\left(r_{i,j}^{true}\left(T_u\right) + \phi_{i,j}\frac{\partial r_{i,j}^{true}\left(T_u\right)}{\partial \phi_{i,j}}\right) + p_j^{false}\left(r_{i,j}^{false}\left(T_u\right) + \phi_{i,j}\frac{\partial r_{i,j}^{false}\left(T_u\right)}{\partial \phi_{i,j}}\right)\right]$$
$$+ \frac{T_d}{T}\left[p_j^{true}\left(r_{i,j}^{true}\left(T_d\right) + \phi_{i,j}\frac{\partial r_{i,j}^{true}\left(T_d\right)}{\partial \phi_{i,j}}\right) + p_j^{false}\left(r_{i,j}^{false}\left(T_d\right) + \phi_{i,j}\frac{\partial r_{i,j}^{false}\left(T_d\right)}{\partial \phi_{i,j}}\right)\right] + \vartheta_i\beta\frac{T_{c,e}}{T}N - \xi_j \quad (38)$$

Let

$$\varpi_{i,j} = \frac{T_u}{T}\left[p_j^{true}\left(r_{i,j}^{true}\left(T_u\right) + \phi_{i,j}\frac{\partial r_{i,j}^{true}\left(T_u\right)}{\partial \phi_{i,j}}\right) + p_j^{false}\left(r_{i,j}^{false}\left(T_u\right) + \phi_{i,j}\frac{\partial r_{i,j}^{false}\left(T_u\right)}{\partial \phi_{i,j}}\right)\right]$$
$$+ \frac{T_d}{T}\left[p_j^{true}\left(r_{i,j}^{true}\left(T_d\right) + \phi_{i,j}\frac{\partial r_{i,j}^{true}\left(T_d\right)}{\partial \phi_{i,j}}\right) + p_j^{false}\left(r_{i,j}^{false}\left(T_d\right) + \phi_{i,j}\frac{\partial r_{i,j}^{false}\left(T_d\right)}{\partial \phi_{i,j}}\right)\right] + \vartheta_i\beta\frac{T_{c,e}}{T}N \quad (39)$$

In order to maximize the system throughput, different channel assignments are compared, and the result that maximizes $\varpi_{i,j}$ is the optimal channel assignment; hence, the expression for $\phi_{i,j}^*$ can be reformulated as:

$$\phi_{i,j}^* = \begin{cases} 0 & \text{other} \\ 1 & \text{argmax } \varpi_{i,j} \end{cases} \quad (40)$$

After determining the optimal $\varphi_{i,j,u}^*$, $\varphi_{i,j,d}^*$, $P_{i,j,u}^{1*}$, $P_{i,j,d}^{1*}$, and $\phi_{i,j}^*$ using the above method, the values for the Lagrangian variable for the kth iteration can be obtained based on the principle of the gradient descent method, which is described as follows:

$$\lambda_j^{k+1} = \left[\lambda_j^k + \alpha_1^k \nabla_{\lambda_j^k} f\left(\lambda_j^k, \chi_j^k, \omega^k, \theta_i^k, \vartheta_i^k, \xi_j^k\right)\right]^+$$

$$\chi_j^{k+1} = \left[\chi_j^k + \alpha_2^k \nabla_{\chi_j^k} f\left(\lambda_j^k, \chi_j^k, \omega^k, \theta_i^k, \vartheta_i^k, \xi_j^k\right)\right]^+$$

$$\omega^{k+1} = \left[\omega^k + \alpha_3^k \nabla_{\omega^k} f\left(\lambda_j^k, \chi_j^k, \omega^k, \theta_i^k, \vartheta_i^k, \xi_j^k\right)\right]^+, \quad (41)$$

$$\theta_i^{k+1} = \left[\theta_i^k + \alpha_4^k \nabla_{\theta_i^k} f\left(\lambda_j^k, \chi_j^k, \omega^k, \theta_i^k, \vartheta_i^k, \xi_j^k\right)\right]^+$$

$$\vartheta_i^{k+1} = \left[\vartheta_i^k + \alpha_5^k \nabla_{\vartheta_i^k} f\left(\lambda_j^k, \chi_j^k, \omega^k, \theta_i^k, \vartheta_i^k, \xi_j^k\right)\right]^+$$

where $[x]^+ = \max(x, 0)$ and $\alpha_1^k, \alpha_2^k, \alpha_3^k, \alpha_4^k, \alpha_5^k$ denote the step size of the kth iteration, which are both set to constants less than zero, and the superscript k denotes the kth iteration. Additionally, $\nabla_x f(x, y)$ represents the partial derivative of $f(x, y)$ with respect to x.

The five partial derivatives in Eq. (41) can be computed as:

$$\nabla_{\lambda_j^k} f\left(\lambda_j^k, \chi_j^k, \omega^k, \theta_i^k, \vartheta_i^k, \xi_j^k\right) = I_{\max,j,d} - \frac{T_d}{T}p_j^{false}\sum_{i=1}^{D} g_{i,j}\varphi_{i,j,d}^* \quad (42)$$

$$\nabla_{\chi_j^k} f\left(\lambda_j^k, \chi_j^k, \omega^k, \theta_i^k, \vartheta_i^k, \xi_j^k\right) = I_{\max,j,u} - \frac{T_u}{T}p_j^{false}\sum_{i=1}^{D} l_{i,j}\varphi_{i,j,u}^* \quad (43)$$

$$\nabla_{\omega^k} f\left(\lambda_j^k, \chi_j^k, \omega^k, \theta_i^k, \vartheta_i^k, \xi_j^k\right) = P_{\max,d} - \frac{T_d}{T}\sum_{i=1}^{D}\sum_{j=1}^{C}\left(p_j^{true} + p_j^{false}\right)\varphi_{i,j,d}^* \quad (44)$$

$$\nabla_{\theta_i^k} f\left(\lambda_j^k, \chi_j^k, \omega^k, \theta_i^k, \vartheta_i^k, \xi_j^k\right) = P_{\max,i,u} - \frac{T_u}{T} \sum_{j=1}^{C} \left(p_j^{true} + p_j^{false}\right) \varphi_{i,j,u}^* \tag{45}$$

$$\nabla_{\vartheta_i^k} f\left(\lambda_j^k, \chi_j^k, \omega^k, \theta_i^k, \vartheta_i^k, \xi_j^k\right) = -E_{\min,i} + \sum_{j=1}^{C} \beta \frac{T_{c,e}}{T} \left(h_{i,j}\left(p_j^{true} + p_j^{false}\right) \varphi_{i,j,d}^* + N\right) \tag{46}$$

The new Lagrangian variables obtained by Eqs. (41)–(46) are compared with the old values, and the iteration ends when it satisfies Eq. (47). Otherwise, the gradient descent step is repeated. Notably, $||x||_2$ denotes the two-parametric number of x.

$$\begin{aligned}
\left\| \lambda_j^{k+1} - \lambda_j^k \right\|_2 &\le \varepsilon_1 \\
\left\| \chi_j^{k+1} - \chi_j^k \right\|_2 &\le \varepsilon_2 \\
\left\| \omega^{k+1} - \omega^k \right\|_2 &\le \varepsilon_3, \\
\left\| \theta_i^{k+1} - \theta_i^k \right\|_2 &\le \varepsilon_4 \\
\left\| \vartheta_i^{k+1} - \vartheta_i^k \right\|_2 &\le \varepsilon_5
\end{aligned} \tag{47}$$

where ε_1, ε_2, ε_3, ε_4 and ε_5 represent the maximum tolerable error for each of the five Lagrangian variables.

Based on the above mentioned process, the overall flow of the SIATS algorithm is described as follows:

Algorithm 1: SIATS algorithm

Input	Number of IoDs in the BS_1 communication range D, iteration step size $\alpha_1^k, \alpha_2^k, \alpha_3^k, \alpha_4^k, \alpha_5^k$, and maximum tolerable error $\varepsilon_1, \varepsilon_2, \varepsilon_3, \varepsilon_4, \varepsilon_5$
Output	Optimal sensing time t_s^*, optimal time allocation factor α^*, and optimal time slot allocation parameters m^* and n^*

1   **for** $t_s \in (0, T]$ **do**
2   **for** $\alpha \in (0, 1]$ **do**
3   Initialize the Lagrangian variables λ_j, χ_j, ω, θ_i, ϑ_i, and ξ_j;
4   Determine the channel gain that matches the exponential distribution $h_{i,j}$, $g_{i,j}$, and $l_{i,j}$;
5   Calculate the false alarm probability $p_{error,j}$ using Eq. (7);
6   Calculate the probability of the first case p_j^{true} using Eq. (6);
7   Calculate the probability of the second case p_j^{false} using Eq. (11);
8   **for** $m \in [1, 3]$ **do**
9   **for** $n \in [1, 4]$ **do**
10   **while** unsatisfied Eq. (47) **do**
11   Calculate the optimal uplink transmit power $P_{i,j,u}^{1*}$ using Eq. (32) and the definition of auxiliary variables;
12   Calculate the optimal downlink transmit power $P_{i,j,d}^{1*}$ using Eq. (35) and the definition of auxiliary variables;
13   Calculate the optimal channel assignment $\phi_{i,j}^*$ using Eqs. (39) and (40);
14   Update the Lagrangian variables using Eqs. (41)–(45);
15   **end while**
16   Calculate the throughput using Eq. (25);

(Continued)

Algorithm 1: (Continued)	
17	**end for**
18	**end for**
19	Compare the throughput with different time slot allocation parameters and obtain the optimal time slot allocation parameters m^* and n^*;
20	**end for**
21	Compare the throughput with different time allocation factors and obtain the optimal time allocation factor α^*;
22	**end for**
23	Compare the throughput with different sensing times to obtain the optimal sensing time t_s^*.

The complexity of the SIATS algorithm proposed in this paper is jointly determined by the cyclic iterations of the four pre-set parameters and the Lagrangian dual problem iterations. The complexity of the four pre-set parameters sensing time t_s, time allocation factor α, and time slot allocation parameters m and n iterations is $O(12T/\iota_t\iota_\alpha\iota_m\iota_n)$, where ι_t, ι_α, ι_m, and ι_n represent the iteration step size of t_s, α, m, and n, respectively. And the complexity of the Lagrangian dual problem iteration is $O(CDG)$, where G represents the number of iterations of the Lagrangian dual problem. Therefore, the complexity of the whole algorithm is $O(12TCDG/\iota_t\iota_\alpha\iota_m\iota_n)$.

4 Simulation Results and Analysis

In this section, the effectiveness of the SIATS algorithm is verified using simulations. During the simulation, it is assumed that all channels in the system conform to the Rayleigh fading channel model [29–31] and that the channel gains follow an exponential distribution. It is also assumed that a total of eight channels are available for the IoDs in the entire system. Some of the parameter settings referred to in this section have been reported previously [32–35], and the specific parameter values are listed in Table 1.

Table 1: Simulation parameters

| Parameters	Values
Time slot duration T	0.1 s
Number of channels C	8
Number of IoDs within the BS_1 communication range D	8,7,6,5
Sampling frequency f_s	6 MHz
Target detection probability p_p	0.9
Energy efficiency conversion constant β	0.7
Probability of CH_j being idle $p\left(H_j\left(0\right)\right)$	0.8
Maximum transmit power of $IoD1_i$ $P_{\max,i,u}$	2.5 W
Maximum transmit power of BS_1 $P_{\max,d}$	10 W
Transmit power of $IoD2_i$ $P_{i,j,u}^2$	2.5 W
Transmit power of BS_2 $P_{i,j,d}^2$	10 W
Maximum uplink interference $I_{\max,j,u}$	0.025 W
Maximum downlink interference $I_{\max,j,d}$	0.1 W
Minimum energy harvested by $IoD1_i$ $E_{\min,i}$	0.01 W
Additive Gaussian white noise variance N	1

(Continued)

Table 1 (continued)

Parameters	Values
Channel gain between BS_1 and $IoD1_i$ $h_{i,j}$	$\sim E(1)$
Channel gain between BS_1 and $IoD2_i$ $g_{i,j}$	$\sim E(0.1)$
Channel gain between BS_2 and $IoD1_i$ $l_{i,j}$	$\sim E(0.1)$
Signal-to-noise ratio of the signals communicated through CH_j SNR_j	$-20, -15, -19, -18,$ $-16, -17, -16, -15$ dB

The simulation is performed for four cases in which the number of IoDs within the communication range of BS_1 communication range are 8, 7, 6, and 5. For the convenience of subsequent calculations, the channel bandwidth is fixed at 1 Hz, therefore, the unit of throughput is expressed as bit/s/Hz [36].

Moreover, the throughput and energy harvesting results obtained during the simulation using the proposed SIATS and FTS algorithms are compared in this study.

The time slot structure in the FTS algorithm is shown in Fig. 3, and it consists of periods for sensing, uplink information transmission, downlink information transmission, and energy harvesting. The total duration of the time slot is T, where the first time period is used for sensing whose duration is t_s. The remaining duration $T - t_s$ is divided into three time periods of equal duration $(T - t_s)/3$, denoted as t_1, t_2, t_3. The time period t_1 is used for the uplink information transmission, and the time period t_2 is used for the downlink information transmission. The time period t_3 is similar to the time period t_L in the SIATS algorithm and is split by the time allocation factor α. The time period αt_3 is used for energy harvesting, and the time period $(1 - \alpha) t_3$ is used for the downlink information transmission.
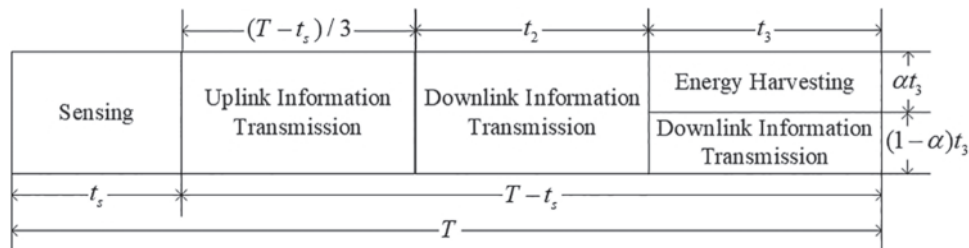

Figure 3: Fixed time slot structure

During the simulation, several scenarios may occur when performing the channel assignments. Fig. 4 shows one of the possible scenarios when the number of IoDs within the communication range of BS_1 is 8, 7, 6, and 5. The horizontal coordinates in Fig. 4 represent the channel number, and the vertical coordinates represent the IoD number. The shaded cells in the figure indicate that the corresponding channel is assigned to the IoD, while the blank cells indicate that the corresponding channel is not available for use by the IoD. For example, in Fig. 4a, the first row indicates that CH_1 is used by $IoD1_6$ and the third row indicates that CH_3 is used by $IoD1_2$.
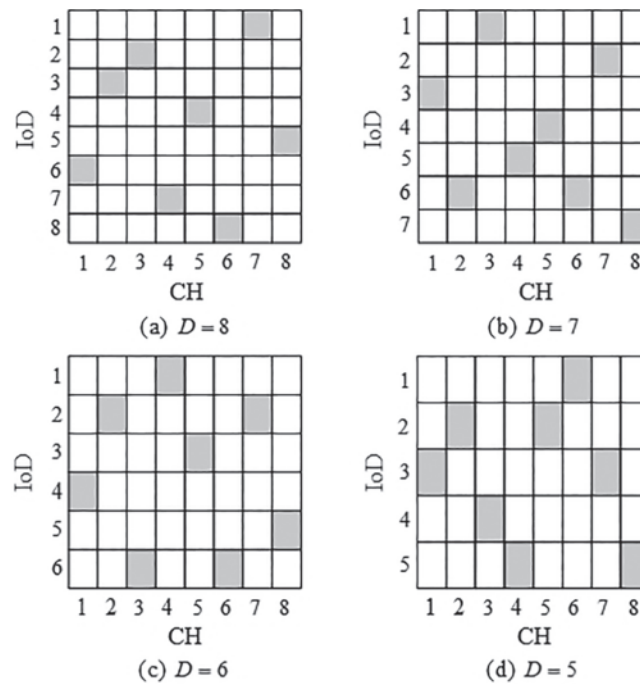
Figure 4: Example of channel assignment. (a) Number of IoDs $D = 8$; (b) Number of IoDs $D = 7$; (c) Number of IoDs $D = 6$; and (d) Number of IoDs $D = 5$

Fig. 5 presents a comparison of the variation in the system throughput with sensing time obtained using the proposed SIATS algorithm with that obtained using FTS algorithm. The horizontal coordinate represents the sensing time, and the vertical coordinate represents the total throughput of all IoDs within the communication range of BS_1. The figure provides a comparison of the total throughput of the proposed SIATS and FTS algorithms for $D = 8, 7, 6$, and 5. The total throughput obtained by using both algorithms with different numbers of IoDs shows a trend of increasing and then decreasing with the increase in the sensing time. The reason for this is that the increase in the sensing time gradually decreases the probability of false alarm, thus increasing the throughput of the system. Additionally, the increase in the sensing time leads to a decrease in the information transmission time that reduces the throughput, thus corresponding to the decreasing trend of the variation. Comparing the curves for the same algorithm for different numbers of IoDs demonstrates that the total throughput increases as the number of IoDs increases, provided that the number of IoDs does not exceed the number of channels. Comparing the curves for different algorithms for the same number of IoDs demonstrates that the throughputs obtained using the SIATS algorithm can be increased by 14.4%, 13.4%, 12.2%, and 10.8% compared with that obtained using the FTS algorithm for $D = 8, 7, 6$, and 5, respectively. The throughput obtained by using the proposed SIATS algorithm is greater than that obtained by using the FTS algorithm, and the proposed algorithm exhibits better performance in terms of the throughput.
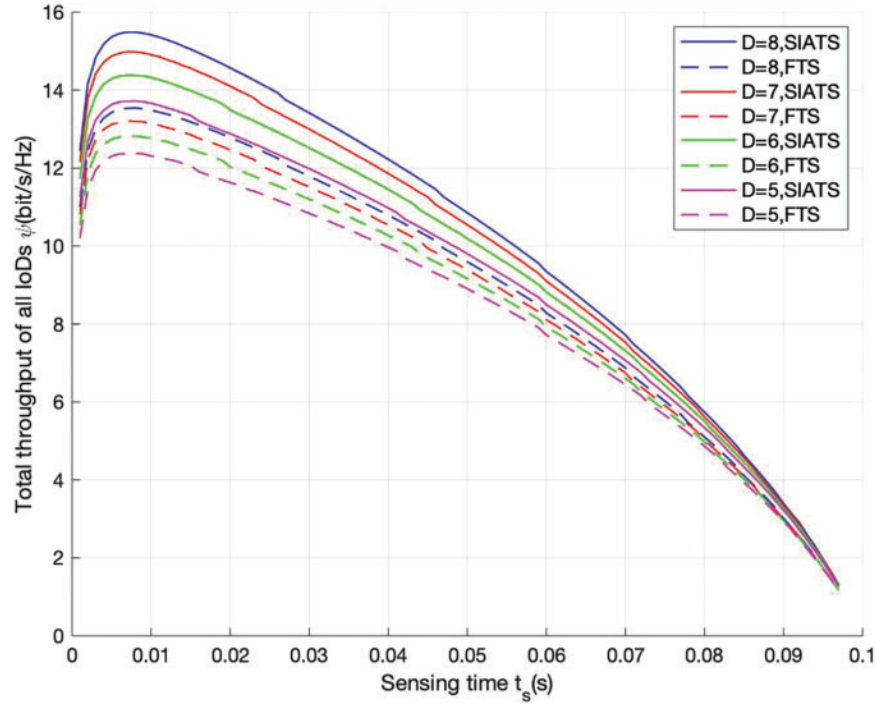
Figure 5: Variation in total throughput of all IoDs within the communication range of BS_1 communication with sensing time

Fig. 6 presents a comparison of the variation in the system throughput with the time allocation factor obtained using the proposed SIATS and FTS algorithms when the sensing time is fixed at t_s = 0.008 s. The horizontal coordinate represents the value of the time allocation factor α, and the vertical coordinate represents the total throughput of all IoDs within the communication range of BS_1. The figure compares the total throughputs obtained using the proposed SIATS algorithm with that obtained using the FTS algorithm for $D = 8, 7, 6,$ and 5. As can be seen from the figure, the total throughput obtained using both algorithms decreases as α increases, because the time allocated to energy harvesting increases as α increases, leading to a decrease in the time available for information transfer, resulting in a decrease in the total throughput. Upon comparing the total throughput results for different algorithms with the same number of IoDs, it can be seen that the proposed SIATS algorithm cannot only obtain a higher total throughput compared with that obtained using the FTS algorithm, but also has a smaller reduction in throughput as the α increases. The reason is that when the value of α is small, the SIATS algorithm increases the time available for energy harvesting by appropriately reducing the proportion of time used for the uplink and downlink information transmissions to ensure that the energy harvesting can meet the system requirements. When the value of α is large, it reduces the time available for energy harvesting by increasing the proportion of time used for uplink and downlink information transmissions, thus significantly increasing the total throughput.
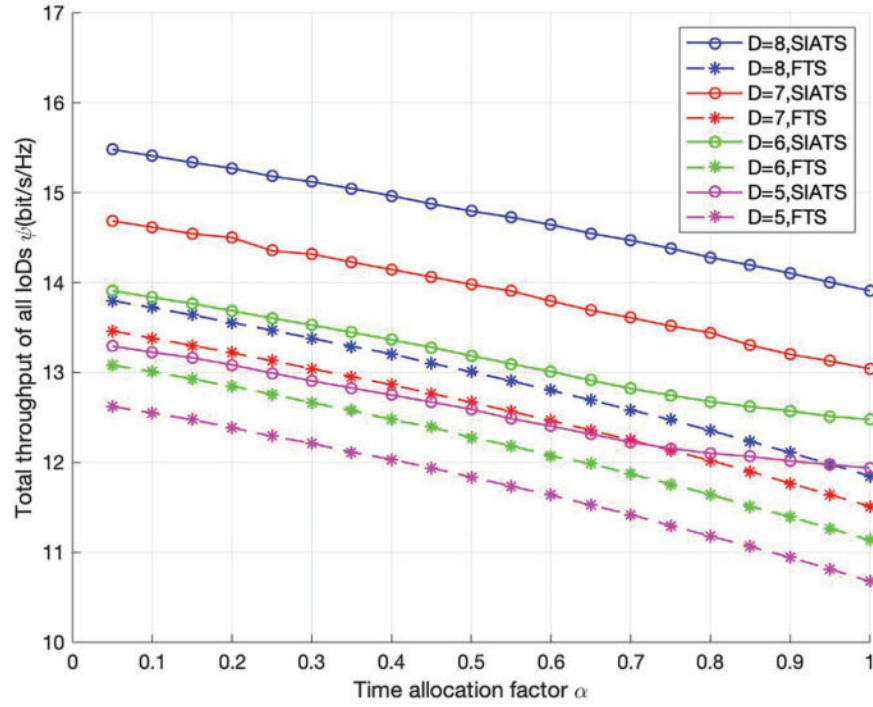
Figure 6: Variation in the total throughput of all IoDs within the communication range of BS_1 with the time allocation factor

Fig. 7 presents the comparison of the energy harvested by each IoD in the proposed SIATS with that in the FTS algorithm when the time allocation factor is fixed at $\alpha = 0.2$. The horizontal coordinate represents the sensing time, and the vertical coordinate represents the energy harvested by the IoD. The figure compares the energy harvesting of the proposed SIATS algorithm with that of the FTS algorithm for the IoD quantities $D = 8$, 7, 6, and 5. From subplots 7a and 7b, it can be seen that the energy harvested by each IoD for $D = 8$ is approximately equal regardless of the value of the sensing time. From subplots 7c and 7d, it can be seen that for $D = 7$, one IoD harvests more energy than the other IoD regardless of the value of sensing time, because one IoD uses two channels while the other IoD uses one channel. Similarly, from subplots 7e, and 7f, it can be observed that because two IoDs use two channels, the two IoDs harvest more energy than the other IoDs for $D = 6$. From subplots 7g and 7h, it can be observed that because three IoDs use two channels, the three IoDs harvest more energy than the other IoDs for $D = 5$. Comparing the energy harvesting results of the SIATS and FTS algorithms for the same number of IoDs, it can be seen that although both algorithms can fulfill the requirements for the predefined minimum energy harvesting, the energy harvested by the IoDs for the SIATS algorithm is significantly less than that for the FTS algorithm. This is because the SIATS algorithm can fulfill the energy harvesting requirement by reducing the proportion by reducing the proportion of time shared between energy harvesting and downlink information transmission and by allocating more time to information transmission, thus obtaining a higher throughput.
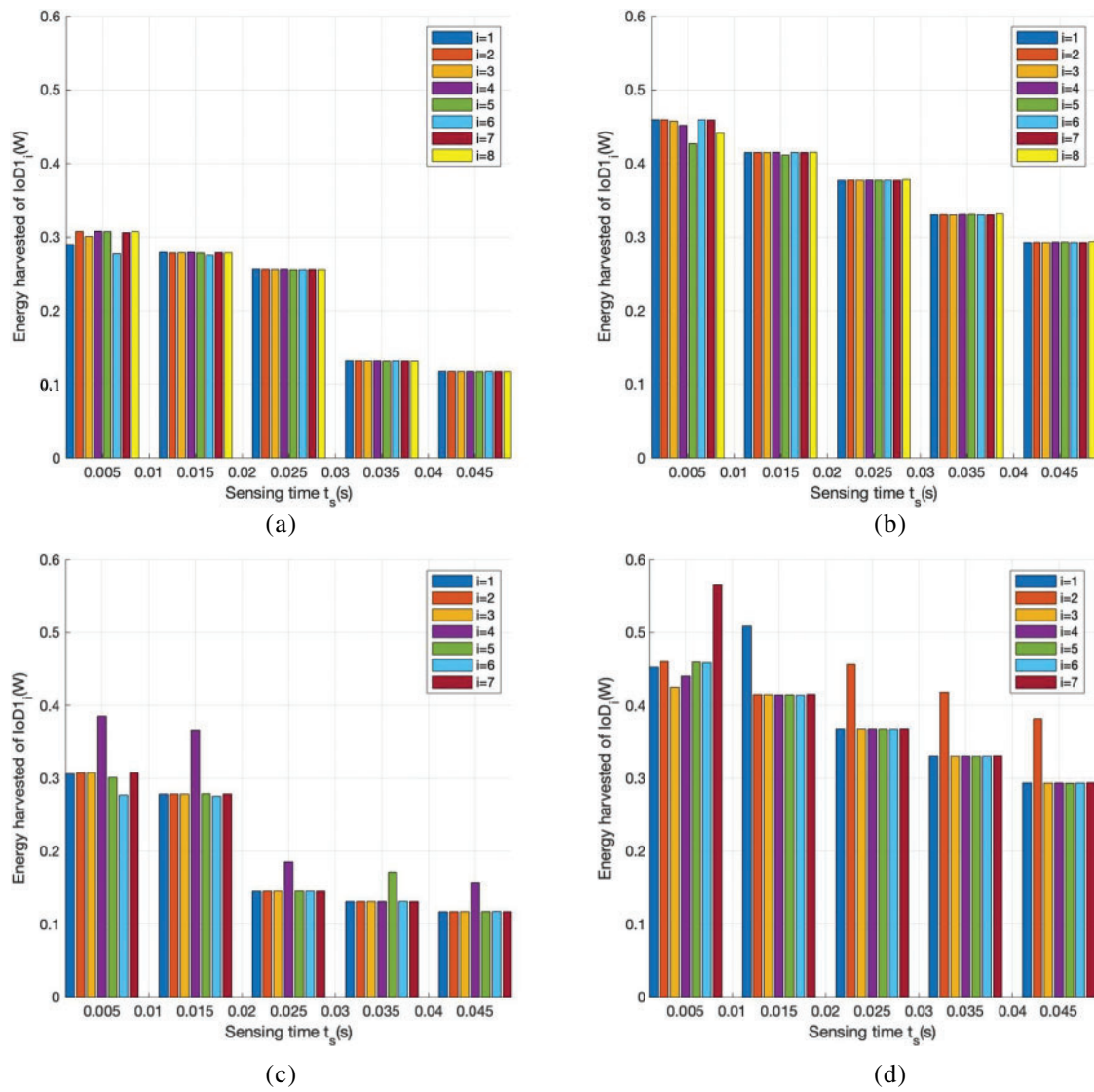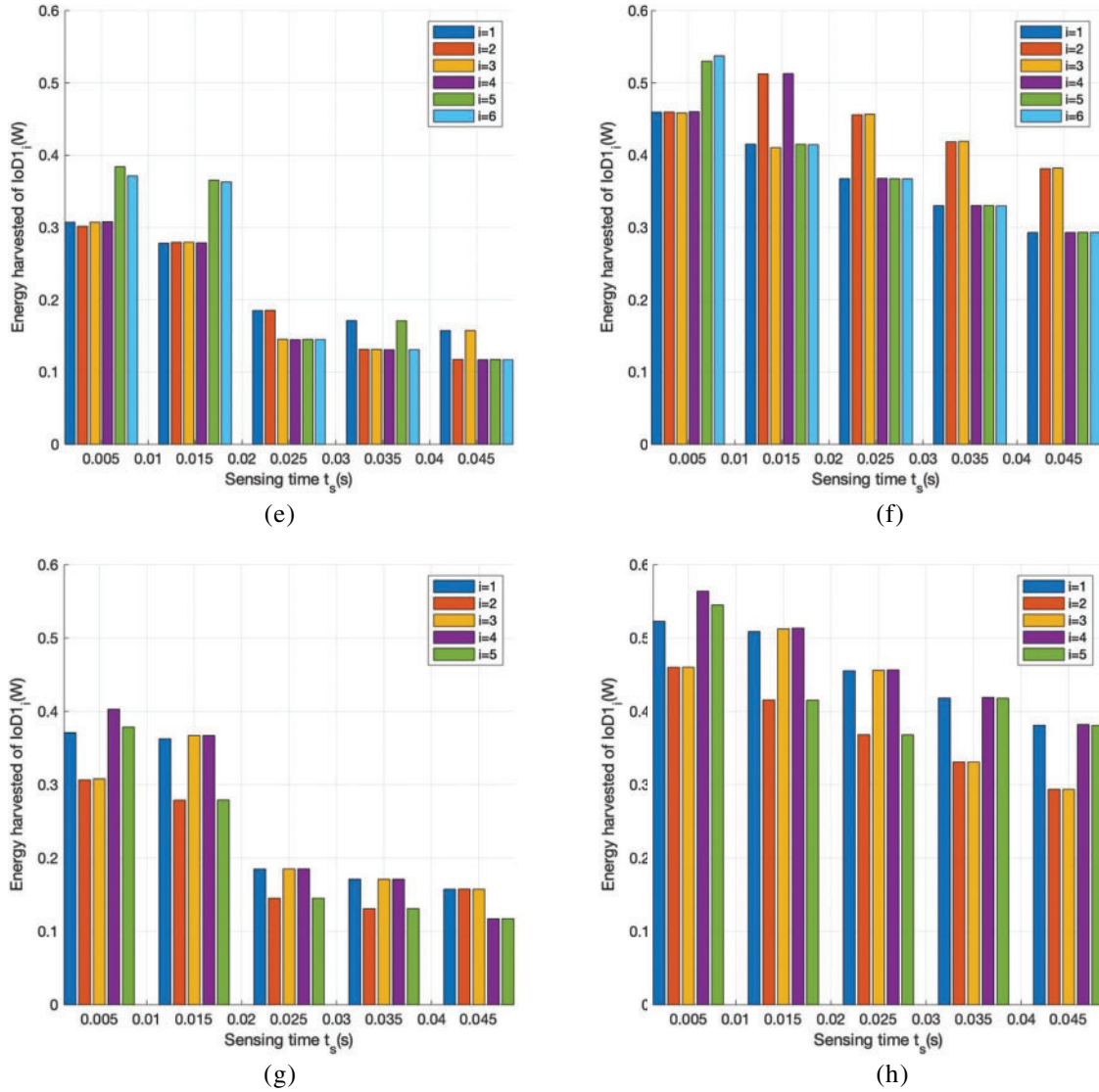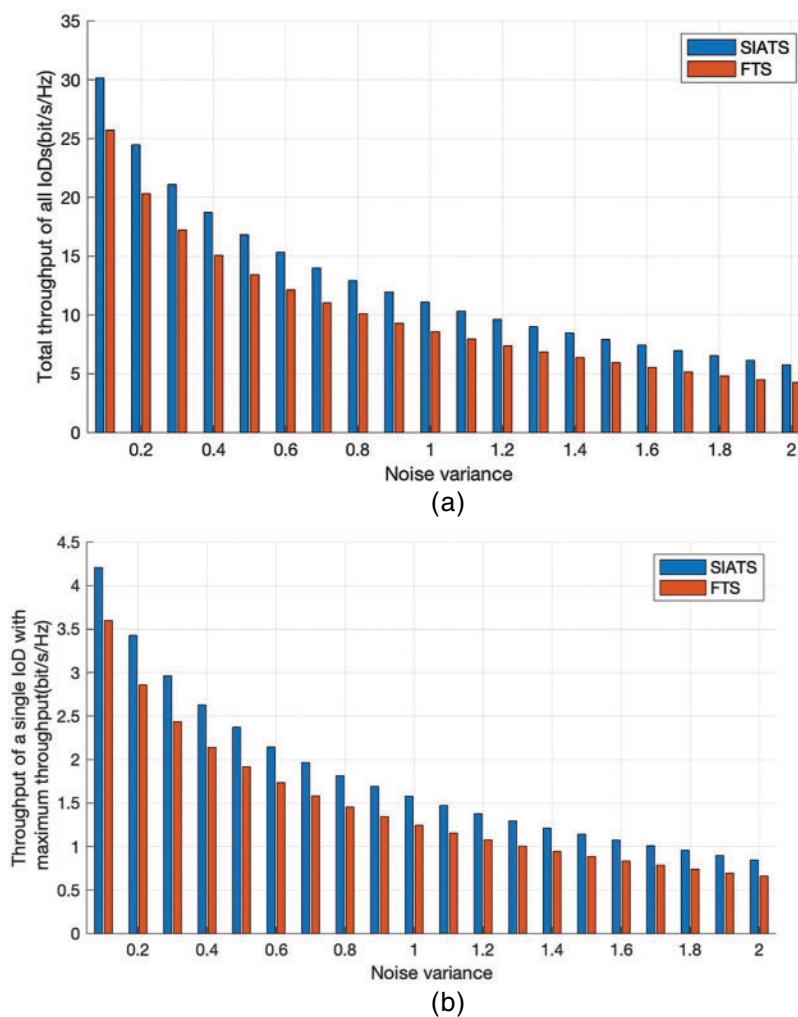
Figure 7: (Continued)

Figure 7: Energy harvesting for IoDi. (a) $D = 8$, SIATS algorithm; (b) $D = 8$, FTS algorithm; (c) $D = 7$, SIATS algorithm; (d) $D = 7$, FTS algorithm; (e) $D = 6$, SIATS algorithm; (f) $D = 6$, FTS algorithm; (g) $D = 5$, SIATS algorithm; and (h) $D = 5$, FTS algorithm

Fig. 8 presents a comparison for the total throughput of all IoDs, the throughput of a single IoD with maximum throughput, and the throughput of a single IoD with minimum throughput for different noise variances obtained by using the proposed SIATS algorithm and FTS algorithms. In the figure, the horizontal coordinates represent the Gaussian white noise variance, and the vertical coordinates represents the throughput. The figure compares the throughput of the proposed SIATS algorithm with that of the FTS algorithm for $D = 8$ and 5. As can be seen from the figures, the total throughput of all IoDs, the throughput of a single IoD with maximum throughput, and the throughput of a single IoD with minimum throughput obtained using the SIATS and FTS algorithms for different numbers of IoDs decrease with increasing noise variance. This is because increasing the noise variance decreases the information transfer rate and thus reduces the throughput. Comparing the results of

the two algorithms, it can be concluded that the total throughput of all IoDs, the throughput of a single IoD with maximum throughput, and the throughput of a single IoD with minimum throughput obtained using the SIATS algorithm are 34.7%, 28.0%, and 33.4% higher than that obtained using the FTS algorithm, respectively, for $D = 8$ and a noise variance of 2. The total throughput of all IoDs, the throughput of a single IoD with maximum throughput, and the throughput of a single IoD with minimum throughput obtained using the SIATS algorithm are 34.0%, 30.9%, and 32.1% higher than that obtained using the FTS algorithm, respectively, for $D = 5$ and a noise variance of 2. The total throughput of all IoDs and the throughputs of a single IoD with maximum throughput, and a single IoD with minimum throughput obtained using the proposed SIATS algorithm are higher compared with that obtained using the FTS algorithm when the noise variance is large. Therefore, it can be concluded that the SIATS algorithm has good noise immunity.

(a)
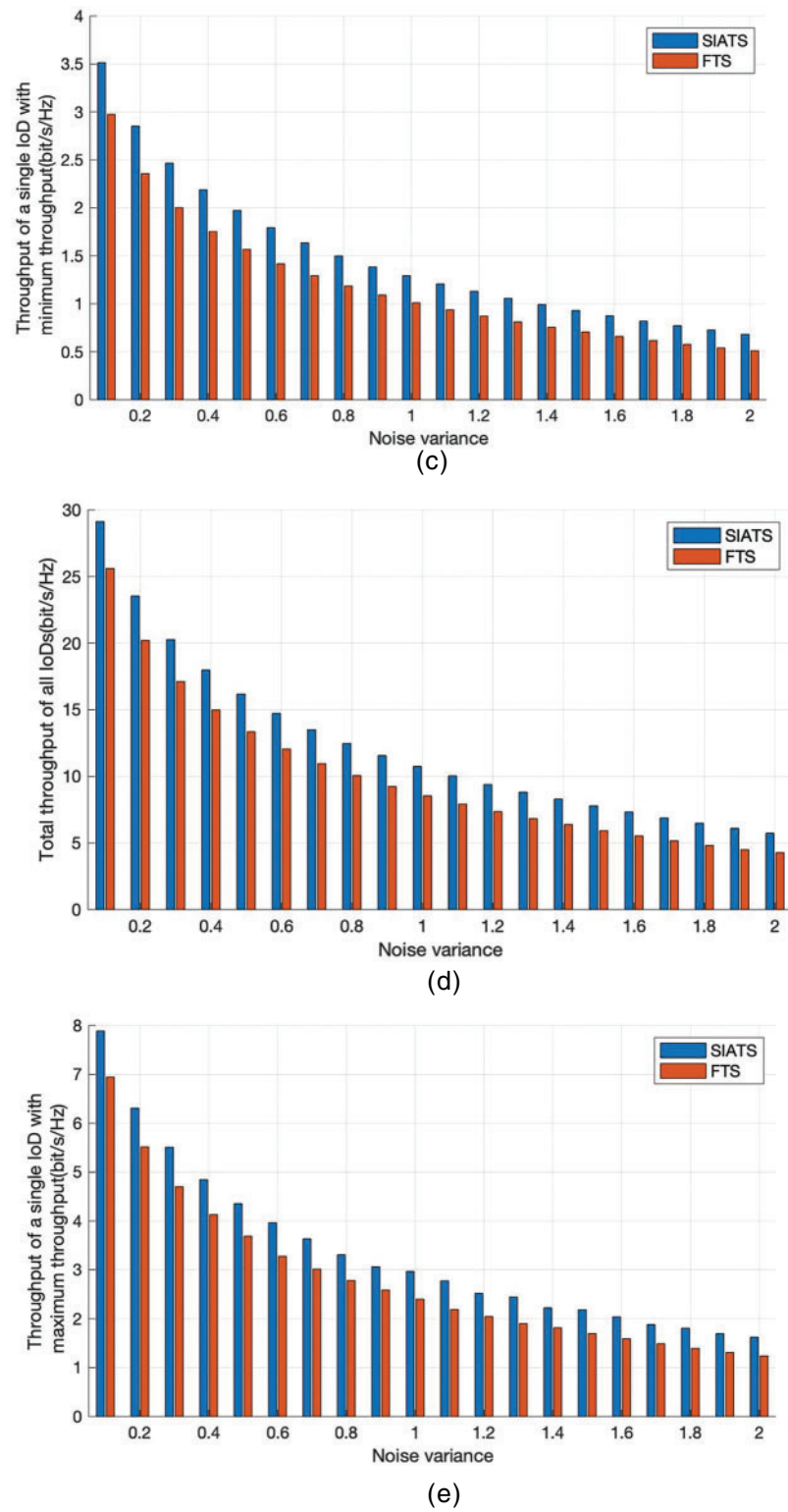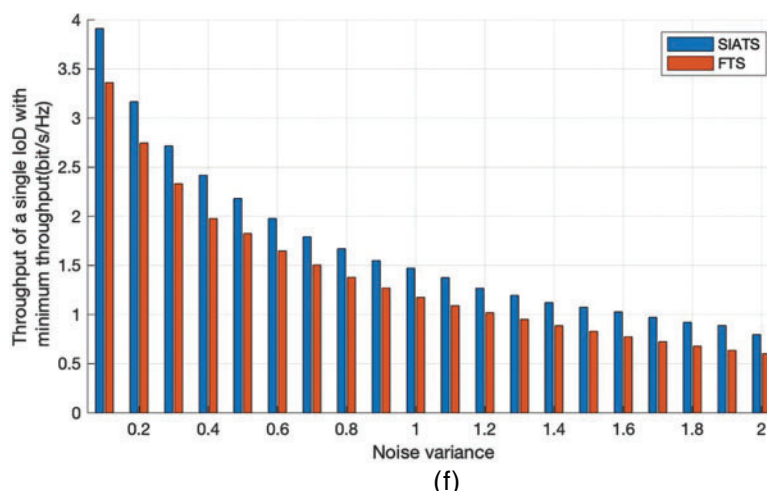

(b)

Figure 8: (Continued)

(c)

(d)

(e)

Figure 8: (Continued)

(f)

Figure 8: IoD throughput at different noise variances. (a) $D = 8$, total throughput of all IoDs; (b) $D = 8$, throughput of a single IoD with maximum throughput; (c) $D = 8$, throughput of a single IoD with minimum throughput; (d) $D = 5$, total throughput of all IoDs; (e) $D = 5$, throughput of a single IoD with maximum throughput; and (f) $D = 5$, throughput of a single IoD with minimum throughput

5 Conclusion

In this study, the SIATS algorithm is proposed to solve the coupling problem in the optimization of resource allocation by using the method of pre-setting the sensing time, time allocation factor, and time slot allocation parameters. Additionally, the optimal transmit power and channel assignment of the system are obtained by using the Lagrangian dual and gradient descent methods. Finally, the optimal time slot parameters of the SIATS algorithm are determined by comparing the throughput results for different values of the sensing time, time allocation factor, and time slot allocation parameters. Simulation results show that the proposed SIATS algorithm performs better, with a maximum throughput improvement of 14.4%, than the FTS algorithm. Meanwhile, by using the SIATS algorithm, the IoD can harvest less energy while satisfying its energy harvesting requirements, thus devoting more time to information transmission. In the case of a large noise variance, the SIATS algorithm displays good noise immunity, and the total throughput of all IoDs obtained using the SIATS algorithm can be improved by up to 34.7% compared with that obtained using the FTS algorithm. Furthermore, throughputs of the best-performing and worst-performing IoDs both improve upon using the proposed SIATS algorithm.

Conflicts of Interest: The authors declare that they have no conflicts of interest to report regarding the present study.

References

1. An, H., Park, H. (2022). Energy-balancing resource allocation for wireless cooperative IoT networks with SWIPT. *IEEE Internet of Things Journal, 9(14),* 12258–12271. https://doi.org/10.1109/JIOT.2021.3135282

2. Sun, L., Wang, Y., Qu, Z., Xiong, N. N. (2022). BeatClass: A sustainable ECG classification system in IoT-based eHealth. *IEEE Internet of Things Journal, 9(10),* 7178–7195. https://doi.org/10.1109/JIOT.2021.3108792

3. Pavani, B., Devi, L. N., Subbareddy, K. V. (2022). Energy enhancement and efficient route selection mechanism using H-SWIPT for multi-hop IoT networks. *Intelligent and Converged Networks, 3(2),* 173–189. https://doi.org/10.23919/ICN.2022.0013

4. Shukla, A. K., Sharanya, J., Yadav, K., Upadhyay, P. K. (2022). Exploiting SWIPT-enabled IoT-based cognitive nonorthogonal multiple access with coordinated direct and relay transmission. *IEEE Sensors Journal, 22(19),* 18988–18999. https://doi.org/10.1109/JSEN.2022.3198627

5. Luo, Y., Pu, L. (2021). Practical issues of RF energy harvest and data transmission in renewable radio energy powered IoT. *IEEE Transactions on Sustainable Computing, 6(4),* 667–678. https://doi.org/10.1109/TSUSC.2020.3000085

6. Sandhu, M. M., Khalifa, S., Jurdak, R., Portmann, M. (2021). Task scheduling for energy-harvesting-based IoT: A survey and critical analysis. *IEEE Internet of Things Journal, 8(18),* 13825–13848. https://doi.org/10.1109/JIOT.2021.3086186

7. Lombardi, M., Pascale, F., Santaniello, D. (2021). Internet of Things: A general overview between architectures, protocols and applications. *Information, 12(2),* 87. https://doi.org/10.3390/info12020087

8. Li, X., Xie, Z., Chu, Z., Menon, V. G., Mumtaz, S. et al. (2022). Exploiting benefits of IRS in wireless powered NOMA networks. *IEEE Transactions on Green Communications and Networking, 6(1),* 175–186. https://doi.org/10.1109/TGCN.2022.3144744

9. Sun, W., Song, Q., Zhao, J., Guo, L., Jamalipour, A. (2022). Adaptive resource allocation in SWIPT-enabled cognitive IoT networks. *IEEE Internet of Things Journal, 9(1),* 535–545. https://doi.org/10.1109/JIOT.2021.3084472

10. Krikidis, I., Timotheou, S., Nikolaou, S., Zheng, G., Ng, D. W. K. et al. (2014). Simultaneous wireless information and power transfer in modern communication systems. *IEEE Communications Magazine, 52(11),* 104–110. https://doi.org/10.1109/MCOM.2014.6957150

11. Kwon, G., Park, H., Win, M. Z. (2021). Joint beamforming and power splitting for wideband millimeter wave SWIPT systems. *IEEE Journal of Selected Topics in Signal Processing, 15(5),* 1211–1227. https://doi.org/10.1109/JSTSP.2021.3089026

12. Liu, Y., Han, F., Zhao, S. (2022). Flexible and reliable multiuser SWIPT IoT network enhanced by UAV-mounted intelligent reflecting surface. *IEEE Transactions on Reliability, 71(2),* 1092–1103. https://doi.org/10.1109/TR.2022.3161336

13. Wang, Y., Yang, K., Wan, W., Zhang, Y., Liu, Q. (2021). Energy-efficient data and energy integrated management strategy for IoT devices based on RF energy harvesting. *IEEE Internet of Things Journal, 8(17),* 13640–14651. https://doi.org/10.1109/JIOT.2021.3068040

14. Ali, A., Feng, L., Bashir, A. K., EI-Sappagh, S., Ahmed, S. H. (2020). Quality of service provisioning for heterogeneous services in cognitive radio-enabled Internet of Things. *IEEE Transactions on Network Science and Engineering, 7(1),* 328–342. https://doi.org/10.1109/TNSE.2018.2877646

15. Zhu, Z., Wang, N., Hao, W., Wang, Z., Lee, I. (2021). Robust beamforming designs in secure MIMO SWIPT IoT networks with a nonlinear channel model. *IEEE Internet of Things Journal, 8(3),* 1702–1715. https://doi.org/10.1109/JIOT.2020.3014933

16. Masood, Z., Park, H., Jang, H. S., Yoo, S., Jung, S. P. et al. (2021). Optimal power allocation for maximizing energy efficiency in DAS-based IoT network. *IEEE Systems Journal, 15(2),* 2342–2348. https://doi.org/10.1109/JSYST.2020.3013693

17. Han, J., Lee, G. H., Park, S., Choi, J. K. (2022). Joint subcarrier and transmission power allocation in OFDMA-based WPT system for mobile-edge computing in IoT environment. *IEEE Internet of Things Journal, 9(16),* 15039–15052. https://doi.org/10.1109/JIOT.2021.3103768

18. Yazdani, H., Vosoughi, A. (2021). Steady-state rate-optimal power adaptation in energy harvesting opportunistic cognitive radios with spectrum sensing and channel estimation errors. *IEEE Transactions on Green Communications and Networking, 5(4),* 2104–2120. https://doi.org/10.1109/TGCN.2021.3087456

19. Xu, Y., Sun, H., Ye, Y. (2021). Distributed resource allocation for SWIPT-based cognitive Ad-hoc networks. *IEEE Transactions on Cognitive Communications and Networking, 7(4),* 1320–1332. https://doi.org/10.1109/TCCN.2021.3068396

20. Qi, Q., Chen, X., Ng, D. W. K. (2020). Robust beamforming for NOMA-based cellular massive IoT with SWIPT. *IEEE Transactions on Signal Processing, 68,* 211–224. https://doi.org/10.1109/TSP.2019.2959246

21. Prathima, A., Gurjar, D. S., Nguyen, H. H., Bhardwaj, A. (2020). Performance analysis and optimization of bidirectional overlay cognitive radio networks with hybrid-SWIPT. *IEEE Transactions on Vehicular Technology, 69(11),* 13467–13481. https://doi.org/10.1109/TVT.2020.3029067

22. Acosta, M. R. C., Moreta, C. E. G., Koo, I. (2021). Joint power allocation and power splitting for MISO-RSMA cognitive radio systems with SWIPT and information decoder users. *IEEE Systems Journal, 15(4),* 5289–5300. https://doi.org/10.1109/JSYST.2020.3032725

23. Tuan, P. V., Koo, I. (2020). Optimizing efficient energy transmission on a SWIPT interference channel under linear/nonlinear EH models. *IEEE Systems Journal, 14(1),* 457–468. https://doi.org/10.1109/JSYST.2019.2924265

24. Hu, C., Li, Q., Zhang, Q., Qin, J. (2022). Security optimization for an AF MIMO two-way relay-assisted cognitive radio nonorthogonal multiple access networks with SWIPT. *IEEE Transactions on Information Forensics and Security, 17,* 1481–1496. https://doi.org/10.1109/TIFS.2022.3163842

25. Tang, J., Yu, Y., Liu, M., So, D. K. C., Zhang, X. et al. (2020). Joint power allocation and splitting control for SWIPT-enabled NOMA systems. *IEEE Transactions on Wireless Communications, 19(1),* 120–133. https://doi.org/10.1109/TWC.2019.2942303

26. Yang, H., Zhong, W., Chen, C., Alphones, A., Du, P. (2020). Deep-reinforcement-learning-based energy-efficient resource management for social and cognitive Internet of Things. *IEEE Internet of Things Journal, 7(6),* 5677–5689. https://doi.org/10.1109/JIOT.2020.2980586

27. Ramzan, M. R., Naeem, M., Altaf, M., Ejaz, W. (2022). Multicriterion resource management in energy-harvested cooperative UAV-enabled IoT networks. *IEEE Internet of Things Journal, 9(4),* 2944–2959. https://doi.org/10.1109/JIOT.2021.3094810

28. Xiao, H., Jiang, H., Shi, F., Luo, Y., Deng, L. et al. (2021). Energy-efficient resource allocation in radio-frequency-powered cognitive radio network for connected vehicles. *IEEE Transactions on Intelligent Transportation Systems, 22(8),* 5426–5436. https://doi.org/10.1109/TITS.2020.3026746

29. Shahini, A., Kiani, A., Ansari, N. (2019). Energy efficient resource allocation in EH-enabled CR networks for IoT. *IEEE Internet of Things Journal, 6(2),* 3186–3193. https://doi.org/10.1109/JIOT.2018.2880190

30. Vu, T., Nguyen, T., Kim, S. (2022). Cooperative NOMA-enabled SWIPT IoT networks with imperfect SIC: Performance analysis and deep learning evaluation. *IEEE Internet of Things Journal, 9(3),* 2253–2266. https://doi.org/10.1109/JIOT.2021.3091208

31. Zhang, Y., He, W., Li, X., Peng, H., Rabie, K. et al. (2022). Covert communication in downlink NOMA systems with channel uncertainty. *IEEE Sensors Journal, 22(19),* 19101–19112. https://doi.org/10.1109/JSEN.2022.3201319

32. Stotas, S., Nallanathan, A. (2011). Optimal sensing time and power allocation in multiband cognitive radio networks. *IEEE Transactions on Communications, 59(1),* 226–235. https://doi.org/10.1109/TCOMM.2010.110310.090473

33. Zhou, F., Li, Z., Cheng, J., Li, Q., Si, J. (2017). Robust AN-aided beamforming and power splitting design for secure MISO cognitive radio with SWIPT. *IEEE Transactions on Wireless Communications, 16(4),* 2450–2464. https://doi.org/10.1109/TWC.2017.2665465

34. Yang, H., Ye, Y., Chu, X., Dong, M. (2020). Resource and power allocation in SWIPT-enabled device-to-device communications based on a nonlinear energy harvesting model. *IEEE Internet of Things Journal, 7(11),* 10813–10825. https://doi.org/10.1109/JIOT.2020.2988512

35. Ma, R., Wu, H., Ou, J., Yang, S., Gao, Y. (2020). Power splitting-based SWIPT systems with full-duplex jamming. *IEEE Transactions on Vehicular Technology, 69(9),* 9822–9836. https://doi.org/10.1109/TVT.2020.3002976

36. Li, G., Liu, H., Huang, G., Li, X., Raj, B. et al. (2021). Effective capacity analysis of reconfigurable intelligent surfaces aided NOMA network. *EURASIP Journal on Wireless Communications and Networking, 198(1),* 1–16. https://doi.org/10.1186/s13638-021-02070-7